

Machine Learning Models to Identify Promising Nested Antiresonance Nodeless Fiber Designs

Rania A. Eltaieb, Sophie LaRochelle and Leslie A. Rusch

Abstract—Hollow-core fibers offer superior loss and latency characteristics compared to solid-core alternatives, yet the geometric complexity of nested antiresonant nodeless fibers (NANFs) makes traditional optimization computationally prohibitive. We propose a high-efficiency, two-stage machine learning framework designed to identify high-performance NANF designs using minimal training data. The model employs a neural network (NN) classifier to filter for single-mode designs (suppression ratio ≥ 50 dB), followed by a regressor that predicts confinement loss (CL). By training on the common logarithm of the loss, the regressor overcomes the challenges of high dynamic range. Using a sparse data set of only 1,819 designs, all with CL greater or equal to 1 dB/km, the model successfully identified optimized designs with a confirmed CL of 0.25 dB/km. This demonstrates the NN has captured underlying physical behavior and is able to extrapolate to regions of lower CL. We show that small data sets are sufficient for stable, high-accuracy performance prediction, enabling the exploration of design spaces as large as $14e6$ cases at a negligible computational cost compared to finite element methods.

Index Terms—Machine learning, Nested Antiresonance Fiber, Truncated Nested Antiresonance Fiber, Hollow core fiber, Confinement loss, Single mode

I. INTRODUCTION

Hollow core fibers (HCFs) have exceptional performance compared with standard solid-core fibers; they offer low dispersion, ultra low nonlinearity and 30% lower latency [1], [2]. While solid core fibers rely on total internal reflection for guidance, HCFs use photonic bandgap or antiresonance reflections [3]–[5]. We focus on antiresonant fibers (ARFs) [4], as they have lower loss, wider bandwidth and less complex structures than photonic bandgap fibers [5].

In ARFs a single layer of hollow capillary tubes in the cladding creates an antiresonant reflection that confines the fundamental mode within the air core. An antiresonant nodeless fiber (ANF) does not allow the tubes to touch one another, eliminating parasitic resonances associated with the glass-to-glass junction. Nesting a small capillary inside each of the main capillaries, nested antiresonant nodeless fiber (NANF), greatly enhances performance. A recent breakthrough in double-nested antiresonant nodeless fibers (DNANFs) [6] resulted in loss < 0.1 dB/km, lower than standard single mode fibers (SMFs).

Previously, we used exhaustive search of the geometric parameters for ANF to find improved designs [7]. The parameter space for NANF or DNANF is much larger than ANF, and the comprehensive search method is impractical. A more efficient, faster method is required.

Machine learning is a powerful tool in the design and modeling of optical components in general [8]–[10], and

optical fibers in particular [11]–[15]. Fiber models allow for accurate prediction of performance metrics, and enable fast numerical optimization algorithms. Machine learning models used for optical fiber design include inverse and direct models.

With machine learning inverse design [11], [12] researchers fix a subset of the fiber design parameters and performance goals. A neural network (NN) is trained to identify the remaining parameters that meet the performance goals. Inverse machine learning has been applied to few mode fibers [11] and ARFs [12]. These models are very difficult to exploit as a great many solutions may meet the performance goals, i.e., the non-unique solution challenge [16].

With machine learning direct models [13]–[15], an NN is trained on the totality of fiber design parameters to predict performance. In [13] the loss of ARFs with a circular and elliptical capillary structure is predicted by an NN. The NN acts as a classifier, mapping a design to a range of confinement loss (CL). Their proposed method used more than 290,000 designs in the data set. A classifier was also used to model a NANF structure in [14], with a data set of 60,000 designs. These approaches were very time consuming due to the size of the data set; each design must be run through a finite element solver. Furthermore, using a classifier does not produce accurate predictions of CL, but only qualitative metrics.

Using regression NNs to predict the CL is challenging due to the wide range of CL values encountered in HCF designs, no matter the data set size. This led to the use of classifiers described previously. Regression NNs were used successfully to predict CL in photonic crystal fibers (with solid core) [15] and NANFs in [17]. The NNs were trained on the logarithm of the dB per length value of confinement loss, which improved the prediction accuracy. However, the single mode guidance is not considered in these models. We apply the logarithmic regression methodology to explicitly identify single mode NANF designs as well as predict CL.

Our research focuses on manufacturable fibers with circular geometry defined by a 4-dimensional parameter space. This contrasts with [17] that employed convolutional neural networks (CNNs) to predict CL using a structured multi-dimensional array of size $16 \times 2 \times 3$ to represent diverse ARF structures including NANF. In [17], the extensive data set of 78,312 designs included several samples with ultra-low loss. We demonstrate that a sparse data set of only 1,819 designs with a 6×1 input to the NN is sufficient to identify high-performance fibers. Notably, although our training data was limited to a minimum loss of 1 dB/km, our model successfully extrapolated to identify optimized designs with a confirmed CL as low as 0.25 dB/km. Furthermore, our

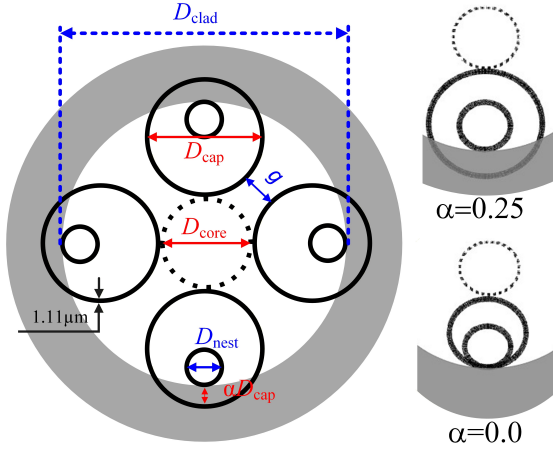


Fig. 1: Parameterization of a NANF geometry with examples of nested nodes for two α .

targeted design space facilitates significantly higher predictive precision, yielding a 5% relative error compared to the 10% relative error reported for the higher-dimensional model [17].

By exploiting NNs to search over an extremely large design space, we achieve performance enhancement at a negligible computational cost compared to finite element methods. We examine prediction accuracy of confinement loss at a central wavelength for various data set sizes and find that even small training sets provide high predictive precision for single-mode NANF optimization.

This paper is organized as follows. We present our NANF geometry, the initial design space, and our strategy for identifying good designs in Section II. We describe the NN structures and the preparation of the data set of different sizes in Section III. We discuss the accuracy of the converged NN models in Section IV. In Section V, we discuss the effectiveness of the NN models to identify promising designs as a function of data set size and search set size. In Section VI we focus on additional factors influencing the performance improvement that we can achieve with our methodology. In Section VII we select one optimized design and show simulation results for confinement loss over an extended wavelength range. Finally, we conclude in Section VIII.

II. FIBERS STUDIED

A. Geometry

On the left of Fig. 1 we sketch a 4-capillary nested antiresonant nodeless fiber (NANF); all structures are circular. Black and gray indicate silica, while white indicates air. The inner cladding diameter is D_{clad} . The four main capillaries have the same inner diameter D_{cap} with uniform gap separation g . The capillaries may penetrate the cladding surface, that is, become embedded in the cladding. We define α as the percentage of the capillary diameter embedded within the cladding. On the right side of the figure, we demonstrate two examples of α . A capillary with an inner diameter D_{nest} is nested inside each main capillary, tangent to the cladding surface (no embedding). The four main capillaries delimit the hollow core diameter D_{core} (dotted circle). All physical dimensions are in μm .

B. Initial Design Space

We select a capillary thickness of $1.11 \mu\text{m}$ for fabrication feasibility and to center the second antiresonance window at 1400 nm (covering the C-band). There remains a vector of four independent parameters fixing a fiber geometry (design): $[D_{core} \ D_{cap} \ \alpha \ D_{nest}]$. The parameters D_{clad} and g are determined by this vector.

With our definition of α , the air space between the nested capillaries is

$$(1 - \alpha) D_{cap} - D_{nest} - 1.11(1 + 2\alpha). \quad (1)$$

Good fiber designs have modes in the main and nested capillaries phase matched. If D_{nest} is too large, the fundamental mode will be lost from the core area and the suppression of all modes will be high. We reject

$$D_{nest} \leq (1 - \alpha) D_{cap} - D_{core}. \quad (2)$$

For reasonable fabrication, we further require D_{nest} to be greater than $0.1(1 - \alpha)D_{cap} \mu\text{m}$.

Our design space is delimited by

$$\begin{aligned} D_{core} &= [20.0 : 1.0 : 60.0], \\ D_{cap} &= [25.8 : 0.5 : 54.3] \\ \alpha &= [0.0 : 0.05 : 0.5] \\ D_{nest} &= [0.1 : 0.05 : 0.6] * (1 - \alpha)D_{cap} \end{aligned} \quad (3)$$

We find the inner cladding diameter D_{clad} for each design per

$$D_{clad} = D_{core} + 2(1 - \alpha)(D_{cap} + 2.22) \quad (4)$$

and the gap g per

$$g = \sin\left(\frac{\pi}{4}\right) D_{core} + \left(\sin\left(\frac{\pi}{4}\right) - 1\right) (D_{cap} + 2.22) \quad (5)$$

We reject designs with

$$g < 3 \ \& \ g > 6. \quad (6)$$

For $g < 3 \mu\text{m}$ there would be high resonance loss; for $g > 6 \mu\text{m}$ there would be high leakage loss. A final check rejects designs where the nested capillary grows large enough to touch the main capillary near the core.

C. Ground Truth Data Set via COMSOL

We identified 18,422 NANF in the design space that respected the conditions in (2) and (6). We used COMSOL to evaluate each design at the center of the antiresonance window studied (1400 nm). From this simulation, we found the confinement loss in dB/km of the fundamental mode (CL) and the first higher order mode (CL^{1st}). We define the suppression ratio, SR , by

$$SR \text{ [dB]} = CL^{1st} \text{ [dB/km]} - CL \text{ [dB/km]} \quad (7)$$

An $SR \geq 50 \text{ dB}$ is a good predictor of single mode behavior.

The lowest CL produced by COMSOL in our data set is 0.276 dB/km . Our goal is to examine the ability of a NN to identify very low loss designs **without having seen those designs in the data set**. For this reason, we excluded 234 designs with CL less than 1 dB/km from the ground truth data set of 18,422 NANFs designs. We reserve these good designs to compare with the NN improved designs in our final remarks.

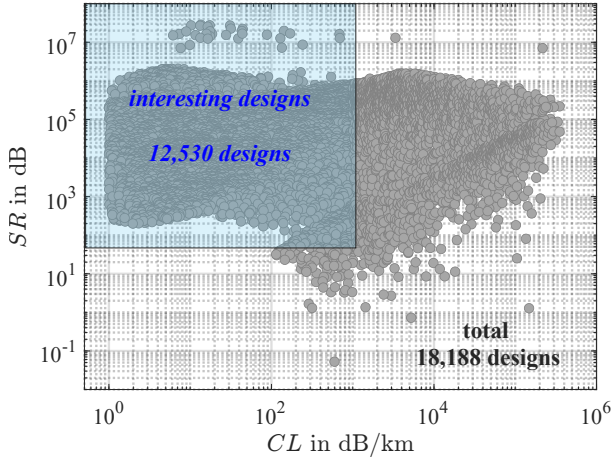


Fig. 2: For the initial design space of 18,188 designs: suppression ratio vs. fundamental mode confinement loss at 1400 nm.

D. Modeling Strategy

We present the scatterplot of confinement loss CL and suppression ratio SR in Fig. 2 for the data set of 18,188 designs. We observe a large dynamic range for both performance metrics. This poses significant challenges for NN models used to predict performance. We can address this issue by adjusting our goals.

The highlighted region in Fig. 2 has 12,530 designs that we label as *interesting*. An interesting design is single mode, which we define as $SR \geq 50$ dB. Furthermore, to be interesting the CL must be less than 10^3 dB/km. Our strategy will be to use a NN classifier to identify that a design is interesting and a NN regression to estimate the CL of the design. In this way, the NN regression faces a much more reasonable dynamic range for performance predication.

The NN model for NANF performance will run orders of magnitude faster than COMSOL and permit a fine search of NANF parameter space. While the classifier passes CL as high as 10^3 dB/km, we will assess regressor performance on designs with CL below 6.3 dB/km. Error in CL prediction above this threshold will not impact the ability to identify a good fiber design (i.e., one at low CL) when searching the NANF parameter space with the NN.

III. NEURAL NETWORK MODEL

In Fig. 3 we show our structure for modeling NANF performance with the goal of identifying fibers with improved performance. *Interesting* designs are identified via a classifier NN. The classifier weights are fixed and designs with a positive classification (interesting) are sent to train a regression NN that estimates the confinement loss of the fundamental mode. The 6-dimensional feature $D = [D_{clad} D_{core} D_{nest} D_{cap} D_{cap}(1-\alpha) g]$ is a single design and is input to both NNs.

A. Data set preparation

The master data set of size $n_{max}=18,188$ designs may be larger than is needed for creation of a good NN predictor

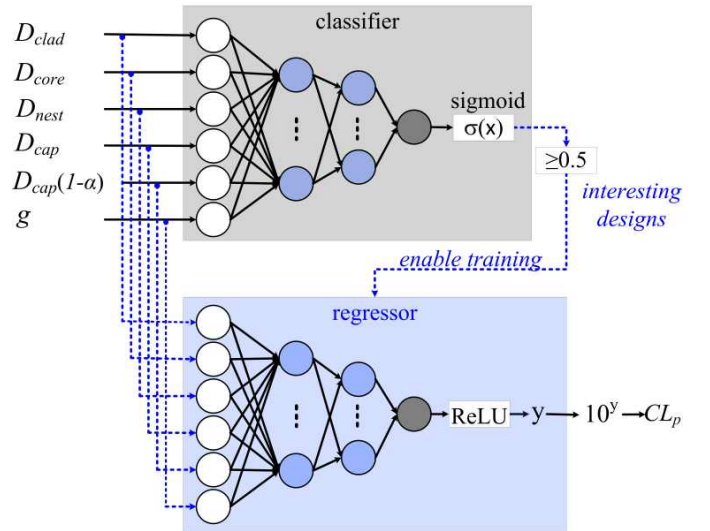


Fig. 3: Classifier and regressor neural network structures for training/testing with dataset of n designs.

of NANF performance. As the simulation time to create the ground truth data is high, we will examine the complexity/accuracy trade-off in data set size. We will set data set size n and randomly select a subset of that size from the master set. Multiple random selections will sometimes be made for a given n .

For each data set of size n , we will randomly partition the set into a training set with 80% of the designs, a validation set with 10% of the designs, and a test set with the remaining 10%. Multiple random partitions will sometimes be made.

B. Classification NN for Identifying Interesting Designs

In Fig. 3 the first stage is a fully connected feedforward NN classifier. The NN classifier has two hidden layers, the first with 70 neurons and the second with 50 neurons. The output layer has one neuron for binary classification to identify an interesting design.

The neuron weights are initialized randomly. We evaluated several activation functions for the hidden layers, and opted for the ReLU function as it offered faster convergence and better performance. We selected the Adam optimizer after evaluating several options.

We use the sigmoid function for the cross-entropy loss function,

$$\sigma(x) = \frac{1}{1 + e^{-x}}. \quad (8)$$

As we have two classes, we threshold the output to achieve the binary classification. The best learning rate we identified was 0.001 for 5000 epochs. A summary of the classifier hyper-parameters is provided in the first column of Table I. Once classifier training is complete, we fix the weights and begin regression training.

C. Regression NN for Confinement Loss Prediction

The regressor NN illustrated in Fig. 3 is a fully connected feedforward NN predicting confinement loss. The entire data

TABLE I: Hyper-parameters of the classifier and regressors

	Classifier	Regressor 1	Regressor 2
# of hidden layers	2	2	2
# of neurons in hidden layers	70, 50	128, 32	130, 38
learning rate	0.001	0.001	0.0001
epoch	5000	5000	10000

set is input to the regression NN, however, weights are only adapted for interesting designs. Inherently, the regression NN sees less data than the classifier NN. Approximately 70% of the designs examined are classified as interesting designs. This percentage depends on our criteria for maximal CL to be considered *interesting*.

The regressor has two hidden layers, each with a distinct numbers of neurons. In Table I we summarize NN hyper-parameters for the classifier and regressors. Data set size had an impact on the best choice for layer size and other hyperparameters. Regressor 1 hyperparameters were used for larger data sets, $n > 9,000$, and regressor 2 hyperparameters were used for smaller data sets, $n \leq 9,000$. We use the ReLU nonlinear activation function to accelerate convergence and enhance performance. We initialize the weights randomly and use the Adam algorithm for faster convergence and improved performance.

We define the true confinement loss as CL_t and the predicted value from the NN regressor as CL_p . Despite reducing the dynamic range of CL_t to 10^3 in the data set, convergence in training is still difficult [15]. We therefore predict the common logarithm of the loss, y , as seen in Fig. 3. The loss is in dB/km, so this is essentially a double logarithm. We convert y to dB/km and report predictions as CL_p in dB/km.

We studied multiple loss functions, and the normalized mean square error (NMSE) loss function showed faster NN regressor convergence. We first estimate the mean square error (MSE) for the training

$$MSE(n) = \frac{1}{0.8n} \sum_{k=1}^{0.8n} (\log_{10}(CL_{t,k}) - y_k)^2 \quad (9)$$

where $0.8n$ reflects training over 80% of a data set of size n . We define mean

$$\mu_t = \frac{1}{0.8n} \sum_{k=1}^{0.8n} (\log_{10}(CL_{t,k})) \quad (10)$$

and variance

$$\sigma_t^2(n) = \frac{1}{0.8n} \sum_{k=1}^{0.8n} (\log_{10}(CL_{t,k}) - \mu_t)^2. \quad (11)$$

The NMSE is therefore as

$$NMSE(n) = \frac{MSE(n)}{\sigma_t^2(n)}. \quad (12)$$

IV. NEURAL NETWORK ACCURACY

In this section we explore the impact of data set size n on NN accuracy in prediction of performance. For data sets with $n \leq 1,500$, our NN overfitted the data or did not converge. We set the smallest data set to examine at $n=1,819$, with eight data set sizes examined in total.

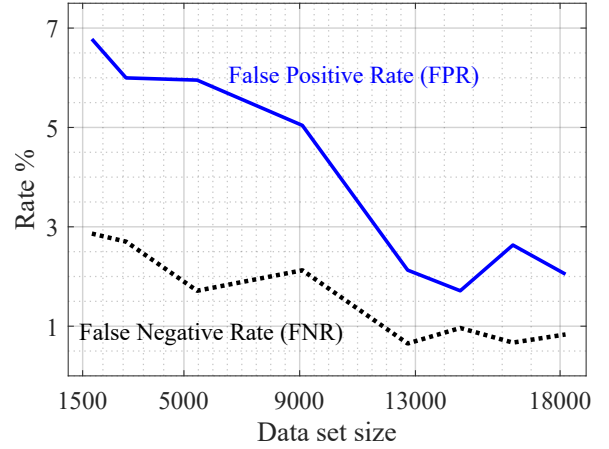


Fig. 4: Classifier false positive and false negative rates vs. data set size.

A. Classification Error for Various Data Set Sizes

We define a trial to be a subset of the master data set and a training/validation/testing partition of that subset. For $n = n_{max}$, the data set is always the master data set; we have ten trials, each a different partition of training/validation/testing. For all other n , the ten trials take the form of ten distinct subsets randomly chosen from the master data set (each with a single partition into training/validation/testing).

For a trial i , the number of true positives is (TP_i); a correctly identified *interesting* design is a true positive. The number of false negatives is (FN_i); an *interesting* design that is incorrectly classified is a false negative. The number of false positives is (FP_i); an unwanted (not interesting) design classified as interesting is a false positive. The number of true negatives is (TN_i); an unwanted design classified as unwanted is a true negative. These four quantities form the confusion matrix for trial i . For each data set size n , we estimate the false negative rate (FNR) and false positive rate (FPR) by averaging over the ten trials

$$\begin{aligned} FNR(n) &= \frac{1}{10} \sum_{j=1}^{10} \frac{FN_j}{FN_j + TP_j} \\ FPR(n) &= \frac{1}{10} \sum_{j=1}^{10} \frac{FP_j}{FP_j + TN_j} \end{aligned} \quad (13)$$

In Fig. 4 we plot the FNR, dashed curve, and FPR, solid curve, rates versus the data set size n . As expected, performance improves (false rates decline) as data set size increases. This improvement saturates from $n=12,732$ onward. Performance at smaller data set size is, nonetheless, acceptable. Even at the smallest n , we identify a minimum of about 97.1% of *interesting designs*. Therefore, we are unlikely to let a good design pass unexamined. The false positive rate is higher (7% rather than 3%), but this will only lead to examining some cases unnecessarily (more computation). Hence, for classification, small data set size is sufficient.

B. Regression Error for Various Data Set Sizes

We quantify regression performance only for designs with relatively low loss. The NN will be exploited to identify good designs, hence its performance for designs with $CL_t \leq 6.3$ dB/km is most relevant. The choice of 6.3 dB/km is ad hoc, but allows for easier visualization and interpretation of results. The training of NN weights covered all designs, affecting convergence. Future work could examine including emphasis on lower loss designs in the training process.

We define absolute relative error ξ as

$$\xi = \left| \frac{CL_t - CL_p}{CL_t} \right|. \quad (14)$$

For a data set of size n , let S_n be the set of designs with $CL_t \leq 6.3$ dB/km collected from the test partition of a trial (trial is as described in the previous section). The average absolute relative error of a given trial, η , is

$$\eta = \frac{1}{|S_n|} \sum_{i=1}^{|S_n|} \xi_i \quad (15)$$

where $|S_n|$ is the number of elements in S_n and ξ_i is the absolute relative error of the i^{th} element of S_n . We define the mean of ξ over ten trials

$$\text{Mean } \xi = \frac{1}{10} \sum_{j=1}^{10} \eta_j \quad (16)$$

In Fig. 5a we plot the estimated mean of average absolute relative error versus the data set size n . The markers indicate the mean values and the error bars represent the standard deviation. Regressor 1 used hyperparameters optimized for larger data set sizes, and regressor 2 used those best for smaller sizes. Both regressors have lower error as data set size grows. In all cases, error is low, never exceeding 0.07 in the mean for designs with $CL \leq 6.3$ dB/km.

We estimated the probability density function (pdf) of the absolute relative error ξ using the kernel method on the normalized histograms from all ten trials [18]. In Fig. 5b, we present the estimated pdf for data sets of size $n=18,188$ and $n=1,819$. The larger data set size has a shorter tail, so better error performance. The means of 0.069 at $n=1,819$ and 0.054 at $n=18,188$ reflect this difference. However, the pdfs are rather similar despite the large difference in data set size.

V. IDENTIFYING BEST DESIGNS

The NN can estimate fiber performance at speeds orders of magnitude greater than what could be accomplished with finite element simulations. In this section, we address the main purpose of the trained NN: searching over an immense design space, identifying a few most promising designs, and then confirming the performance improvement in a finite element simulation. Previous sections reported error over multiple trials of each data set size. Given the time required for confirmation of performance, in this section we restrict our attention to a single trial at each data set size.

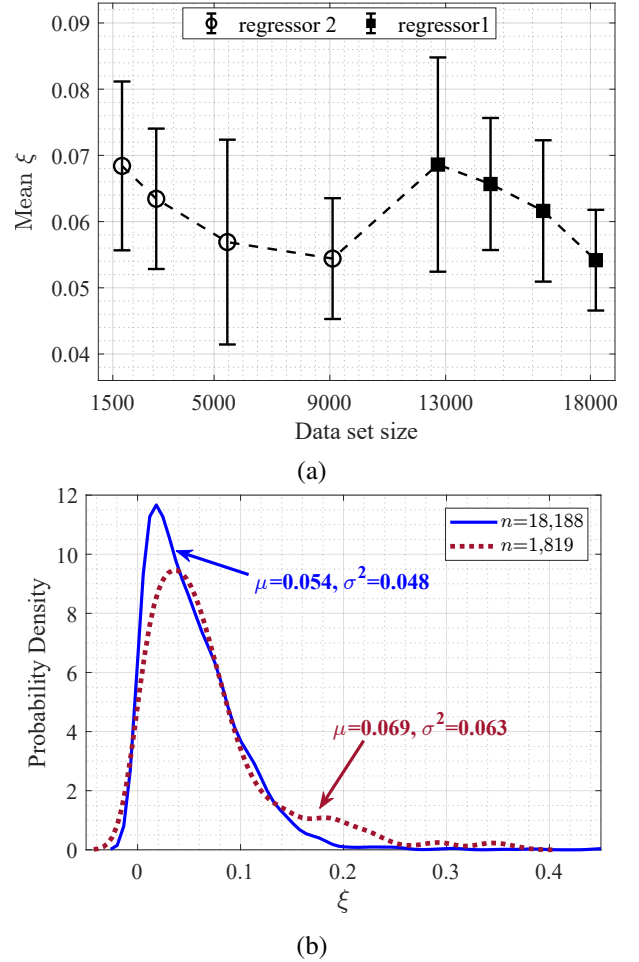


Fig. 5: a) Mean absolute relative error vs. data set size n for designs with $CL \leq 6.3$ dB/km with error bars indicating standard deviation; b) estimated probability density function of the absolute relative error for $n=1,819$ and $n=18,188$.

A. Search Space

We use our trained NN model to explore a space of $N \gg n$ designs, i.e., a much larger and denser space than the data set. We randomly sample the design space with a uniform distribution for D_{core} and D_{cap} parameters in the following ranges:

$$\begin{aligned} D_{core} &\in [20.0: 31.0] \\ D_{cap} &\in [25.8: 54.3] \end{aligned} \quad (17)$$

For each random pair (D_{core}, D_{cap}) we examine a grid of 121 pairs (α, D_{nest}) taken from

$$\begin{aligned} \alpha &= [0.0: 0.02: 0.5] \\ D_{nest} &= [0.1: 0.02: 0.6] * (1 - \alpha) D_{cap} \end{aligned} \quad (18)$$

We discard those designs that do not meet the criteria (2) and (6). We continue to sample (D_{core}, D_{cap}) until $N \sim 14e6$ valid designs have been identified and the loss predicted via NN.

B. Performance Improvement with Large Data Set

We first examine a NN trained with the master data set. The search space of $14e6$ designs yields about $1.2e6$ designs with $CL_p \leq 2.8$ dB/km. The histogram of CL_p for these designs is given in Fig. 6a in gray. The histogram of CL_t from the data set is given in red; 1,139 out of 18,188 designs have $CL_t \leq 2.8$ dB/km.

Consider the far left edge of the gray histogram given in the inset of Fig. 6a. Our NN found 62 designs with $CL_p \leq 0.3$ dB/km. We have put in bold black lines the CL_p for the 18 best designs identified by the NN. We ran COMSOL on these designs to determine CL_t , displayed in bold blue lines in the inset. We limited our examination to 18 designs given the COMSOL simulation time.

Although the master data set had a minimum CL_t of 1 dB/km, searching over a large search space with an NN identified thousands of NANF designs with potentially improved performance. The potential was confirmed with finite element simulations. With this particular trial, the confirmed CL_t is less than the predicted CL_p . We confirmed a design with $CL_t \approx 0.25$ dB/km, greatly improving over the data set at 1 dB/km.

C. Performance Improvement using Small Data Set

We next examine a NN trained with the smallest subset of the master data set. Recall that data sets with $n \leq 1,500$ did not converge or overfitted, hence $n=1,819$ is the smallest data set examined. One subset was selected randomly from the master data set, and the results are presented here.

In Fig. 6b we plot histograms for predicted and true CL, as we did in Fig. 6a for the master data set. The gray histogram has the same density for the two figures as the same search area is covered (size $14e6$). The red histogram is much less dense as only 10% of the master data set is included; for $CL < 2.6$ dB/km there are 126 designs for the small set vs. 1,139 for the large set. In both cases the data set has by construction a minimum $CL_t \approx 1$ dB/km.

The trained NN was able to identify 3646 designs with predicted $CL_p \leq 0.3$ dB/km, as seen in gray in the inset. The lowest CL_p is 0.22 dB/km, with the best 18 designs in black on the inset. The confirmed CL_t of these designs (in blue) show a minimum ≈ 0.25 dB/km. For these two trials, one at n_{min} and one at n_{max} , the confirmed, minimum CL_t are similar. Therefore, it appears that a small data set is sufficient to train a NN to find designs with promising performance at low computational cost. It is interesting that for these particular trials, predictions are optimistic for n_{max} and pessimistic for n_{min} .

D. Impact of Data Set Size

Our examination in the previous section of a small and large data set size showed that the best designs identified in each case led to similar confirmed performance. We continue to examine this behavior over more data set sizes n .

Let D_i be any design in the search space of $M \approx 14e6$ designs. We index the designs according to their predicted

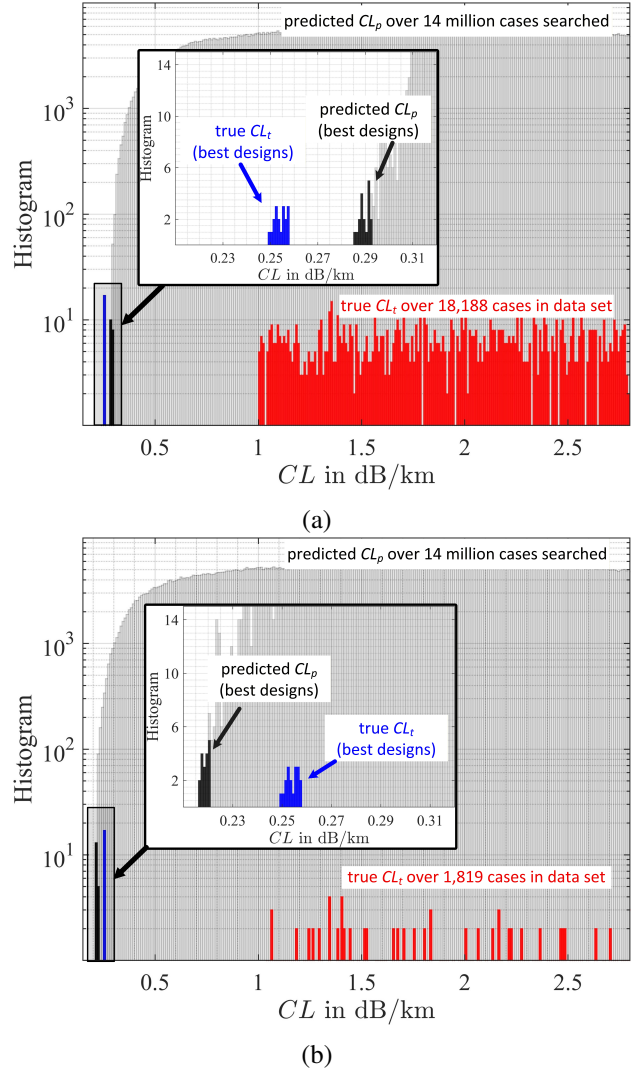


Fig. 6: Histograms of: gray predicted CL_p over search space, red true CL_t over data set; inset has predicted CL_p in bold black, and their confirmed, true CL_t in bold blue, for data sets of size a) $n=18,188$ and b) $n=1,819$.

performance $CL_p(D_i)$. Let D_1 be the best design identified by a given NN, i.e., $CL_p(D_1) \leq CL_p(D_2) \leq \dots \leq CL_p(D_M)$. We examined eight NNs, each at a distinct n and each trained on one trial, i.e., one random subset of the master data set with a random partition into training/validation/testing.

Before plotting, we sorted the NN results along $CL_p(D_1)$. The NN with $n=14,550$ had the design with the lowest minimum predicted loss, and NN with $n=18,188$ had the design with the highest minimum predicted loss. The results are plotted in Fig. 7 in the curve with circle markers; the x -axis specifies n .

The predicted loss varies from 0.18 to 0.29 dB/km for the data sets examined. There is no observable correlation between predicted $CL_p(D_1)$ and data set size. Two large data sets yield the lowest and highest predicted CL, while the smallest data set provides a median value for predicted CL. We also plot in star markers the confirmed loss $CL_t(D_1)$. The variation of confirmed best-case loss, $CL_t(D_1)$, varies from 0.25 to

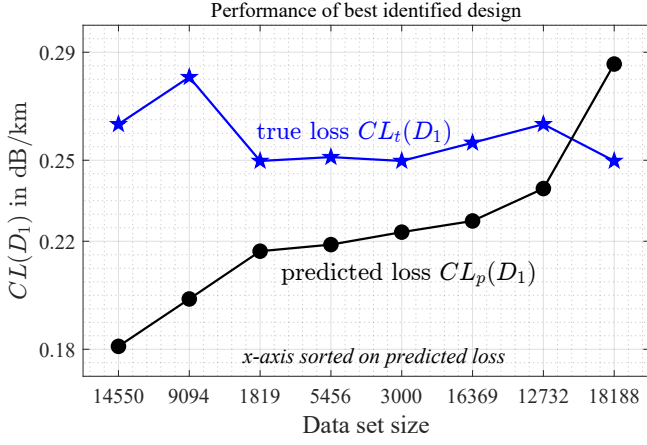


Fig. 7: Confinement loss of the best designs at each data set size; predicted is $CL_p(D_1)$ and confirmed is $CL_t(D_1)$.

0.29 dB/km. While the span of the predicted $CL_p(D_1)$ is 0.11 dB/km, the confirmed $CL_t(D_1)$ has a span of only 0.03 dB/km. Although most predictions were optimistic, the true CL was lower than the predicted CL at $n=18,188$.

Recall the data sets had CL greater than 1 dB/km in all cases. At all data set sizes we see a marked reduction in $CL_t(D_1)$. Therefore, NN are very effective in taking a set of fiber designs with mediocre performance and finding greatly improved designs. The NN approach has computational cost orders of magnitude lower than finite-element methods.

From Fig. 7, we conclude that larger size is not needed to identify designs with greatly improved true CL_t . Furthermore, the error in prediction does not impact the quality of the design. That is, cases where predicted CL_p was overly optimistic still yielded a design with good true CL_t (0.26 dB/km); maximum error of 0.08 dB/km at data set size of 14,550 still maintains low confirmed loss. The NN with the smallest error (NN with data set size 12,732) yields a design with the same true CL_t of 0.26 dB/km. Error is critical in training to get a good NN, but less important when considering the best designs found searching over a very dense design space.

VI. FACTORS IMPACTING PERFORMANCE IMPROVEMENT

In section V, for one trial per n , we examined the NNs performance for 1) a search set of $14e6$ designs, and 2) examination of $CL_t(D_1)$. In section IV we included multiple trials to examine NN error performance. In this section we investigate the impact of these choices.

A. Impact of search set size on NN best designs

In Fig. 7, for each n , we plot $CL_p(D_1)$ that is the minimum predicted CL over the entire search area A with $|A| = 14e6$. In this section, with our compiled data over A , we consider what might have happened had we used a smaller search area. Specifically, we examine how $CL_p(D_1)$ would be impacted. We fix a search size $m \leq M$ and randomly select 50 subsets of that size. Each subset will have a new best design, with a new best predicted CL. We estimate $E[CL_p(D_1)]$ for each m by averaging over the 50 subsets' best predicted CL.

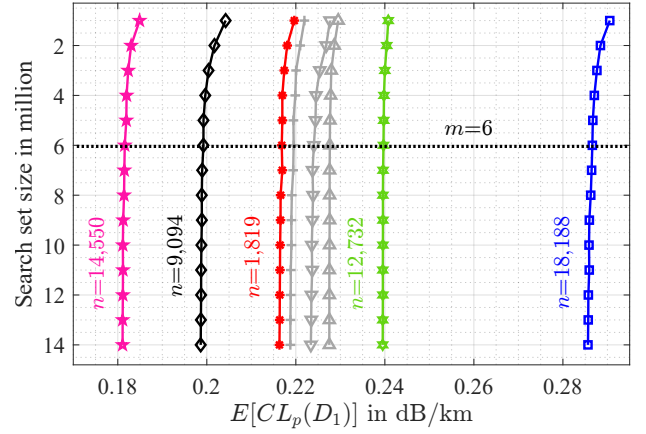


Fig. 8: For each data set size n , search set size in millions versus $E[CL_p(D_1)]$ as estimated over 50 trials.

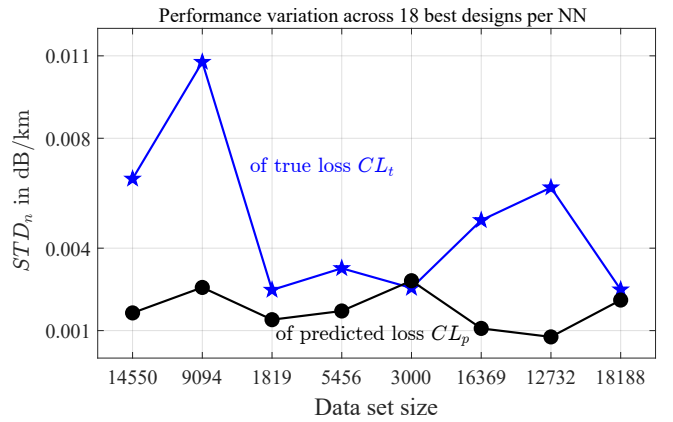


Fig. 9: Standard deviation of the best 18 predicted and confirmed designs at all studied data set sizes.

Figure 8 shows the search set size m versus $E[CL_p(D_1)]$. Each curve refers to a data set of size n for training the NN. The “bottom” of each curve refers to $CL_p(D_1)$ at $m = M$, i.e., the results in Fig. 7.

The curves are very steep, showing that our search set size was much larger than necessary. A search set of $m = 6e6$ is sufficient to identify roughly the same minimal predicted CL. However, the difference in NN execution time for $m = 6e6$ or $m = M = 14e6$ is negligible. Therefore, we continued our studies with the $14e6$ search set.

B. Relevance of Design with Lowest Predicted Loss

In the inset of Fig. 6, we highlighted the performance of a subset of the best designs, both predicted and true. As the confirmed true CL_t required finite element simulation, we limited this group to the 18 best designs. In this section, we examine the variation in predicted and confirmed loss among this group.

For a given NN with a data set size n , we calculate the standard deviation STD_n by

$$STD_n = \sqrt{\frac{1}{17} \sum_{i=1}^{18} (x_i - \bar{x})^2} \quad (19)$$

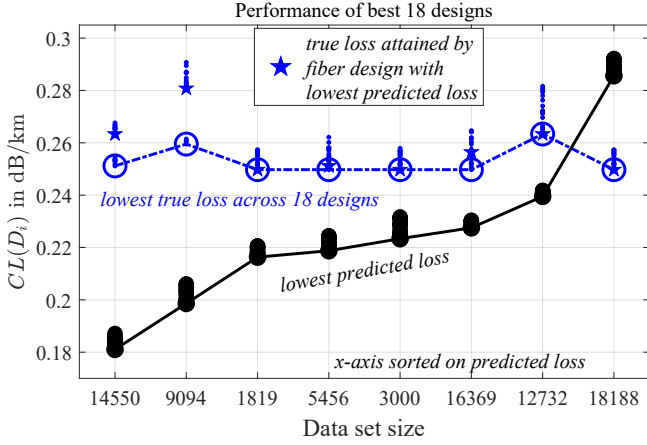


Fig. 10: The best predicted confinement loss CL_p in black dots, their confirmed confinement loss CL_t , and the best confirmed confinement loss among the 18 design validated in COMSOL versus data set size.

where x_i is the confinement loss of design i , and \bar{x} is the mean of the confinement loss of the 18 designs. In Fig. 9, we plot the standard deviation STD_{D_n} versus data set size for CL_t and CL_p . The x -axis has the same ordering as in Fig. 7.

The standard deviation of the predicted and confirmed losses is small, with a maximum value of 0.011 dB/km. In most cases, the standard deviation of the confirmed loss is higher than that of the predicted loss; there is an exception at $n=3,000$.

In Fig. 10, we recreate Fig. 7 and add information on $CL_t(D_i)$, $i \in (2, 18)$. The star markers are $CL_t(D_1)$ whereas the empty circle markers are $\min_i CL_t(D_i)$. All other $CL_t(D_i)$ are dots. The $CL_p(D_i)$ are plotted as filled circles.

The difference in dB/km between star and empty circle markers indicates the improvement in true lowest CL if we use finite element to examine a collection of 18 most promising designs. The difference is small, but could prove worthwhile. Our proposed methodology is to use a few minutes to search with NN and a few hours (in the case of 18 cases) to refine with finite element. Training time of the NN is negligible (included in the few minutes).

C. Impact of Data Set Realization

In section V, we saw in Fig. 7 that the smallest data set could produce good NANF designs. These results were based on a single trial at each data set size n . In this subsection, we investigate multiple trials for $n = n_{min}$ before generalizing our conclusion.

We randomly select 20 subsets of size $n=1,819$. Each subset is divided into a training/validation/testing partition to train an NN. Based on the observations in the previous subsections, we fix the search set of size $M = 14e6$, and we begin by examining only the D_1 design output in each trial. Finally, we examine the statistics of performance of the 18 best designs over all trials.

We sorted the results of the trials, with trial index of one for the lowest $CL_p(D_1)$, and 20 for the highest $CL_p(D_1)$.

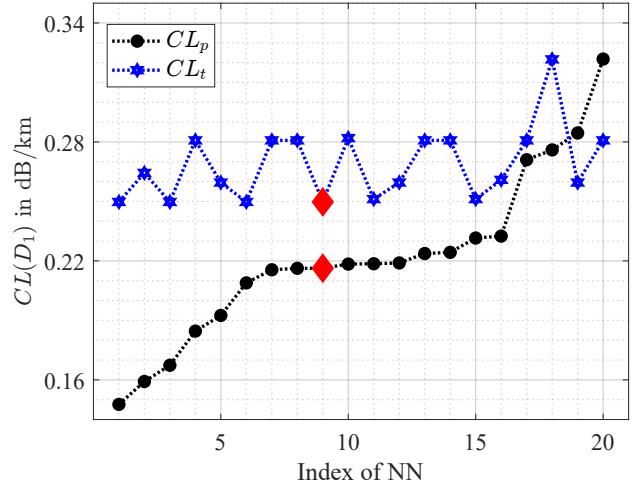


Fig. 11: Confirmed and predicted confinement loss of design 1 versus the NN index with a data set of size $n=1,819$.

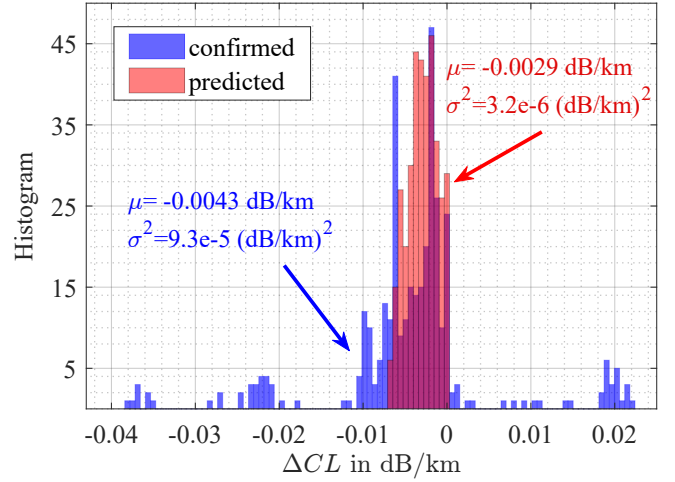


Fig. 12: Histogram of ΔCL for best 18 designs (relative to lowest predicted $CL(D_1)$) for the 20 tested NN models of size $n=1,819$.

In Fig. 11 we plot predicted $CL_p(D_1)$ and confirmed loss $CL_t(D_1)$ versus trial index. The large diamond marker indicates the trial that is reported in all previous results for $n = n_{min}$.

Consider the relative values of $CL_p(D_1)$ and $CL_t(D_1)$. The majority of cases have optimistic predictions, i.e., $CL_p(D_1) < CL_t(D_1)$. Recall that in Fig. 7 only one n showed a pessimistic prediction, $n = n_{max}$. The pessimism may not be related to the size of n ; perhaps it is simply that one of eight trials happened to be pessimistic.

Consider the range of predicted $CL_p(D_1)$ and confirmed $CL_t(D_1)$. The predicted $CL_p(D_1)$ spans 0.15 dB/km, but the confirmed loss $CL_t(D_1)$ only spans 0.05 dB/km. Whether optimistic or pessimistic, whatever design D_1 is found, its true loss indicates a significant improvement over the loss in the data set. We can also consider the distance between the curves (the error), which does not exceed 0.1 dB/km. This is the equivalent of 0.41 relative error per the definition (14). This maximum among the twenty trials would fall in the tail

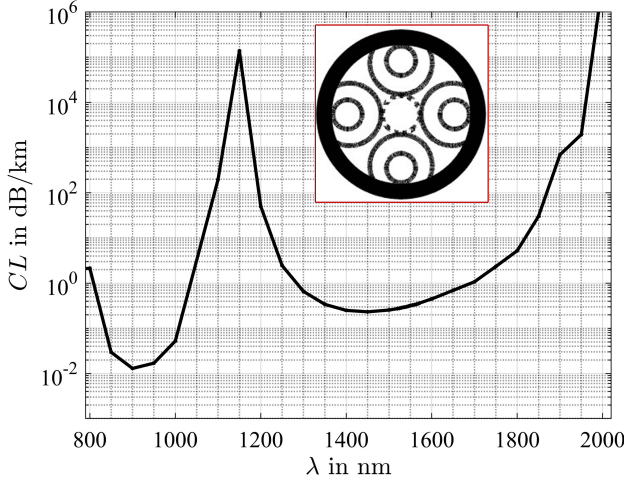


Fig. 13: The confinement loss versus wavelength of the design in red diamond marker in Fig. 11. The inset is a scaled schematic of the fiber structure.

of the estimated pdf in Fig. 5. That pdf was estimated from the sparse test portion of the data set; the much higher granularity of the search set makes it less surprising to fall in the tail of the distribution.

Finally, we consider the statistics of $CL_p(D_j)$ and $CL_t(D_j)$ for $j \in (1,18)$, 360 designs in total. For each design, we compute the error ΔCL , defined by

$$\Delta CL_j = CL(D_1) - CL(D_j). \quad (20)$$

In Fig. 12, we plot the histograms of ΔCL of both predicted and confirmed loss. The histograms are skewed negative, meaning that, for both predicted and confirmed loss, the presumed best case D_1 is likely to truly be the best design. As expected from results in the preceding subsections (see Fig. 9), the predicted loss has a much more compact histogram than the true confirmed loss. The error in prediction is the source of the spread in the true loss. However, the span is still quite low, with a variance of $9.3e-5$ (dB/km)².

VII. DISCUSSION

In the previous sections, we addressed the performance of the best identified designs at 1400 nm. The design yielding the red diamond marker in Fig. 11 had $[D_{core} D_{cap} \alpha D_{nest}]$ of $[31.0 \ 51.8 \ 0.22 \ 24.2]$, with diameters in μm . We study the performance of this design over the two antiresonance windows wavelengths.

In Fig. 13, we plot the fundamental mode confinement versus the wavelength for this design. The inset shows a scaled schematic of the selected NANF structure. Over the C-band, the confinement loss never exceeds 0.4 dB/km. The confinement loss of the design does not exceed 1 dB/km over O-, C-, and L-bands. Despite training our NN model on a data set with performance at 1400 nm, our model was able to identify a good design with stable performance over O-, C-, and L-bands.

VIII. CONCLUSION

In this study, we demonstrated a robust two-stage machine learning architecture for the rapid design and optimization of NANF structures. By decoupling the identification of single-mode behavior from the prediction of confinement loss, our model effectively manages the vast dynamic range of optical performance metrics. The results demonstrate significant data efficiency; a data set of 1,819 designs proved sufficient to accurately navigate a search space of $14e6$ potential geometries. Furthermore, the model was able to identify optimized designs with a confirmed CL of 0.25 dB/km, despite being trained exclusively on data with $CL \geq 1$ dB/km. This suggests that the neural network captures the underlying physical trends of antiresonance guidance rather than merely interpolating within the training bounds. The stability of these findings across multiple data set realizations indicates that the proposed methodology offers a reliable, low-cost alternative to exhaustive finite element simulations, substantially accelerating the design cycle for hollow-core fibers.

REFERENCES

- [1] F. Poletti, "Nested antiresonant nodeless hollow core fiber," *Optics Express*, vol. 22, no. 20, pp. 23 807–23 828, 2014.
- [2] E. Numkam Fokoua, S. Abokhamis Mousavi, G. T. Jasion *et al.*, "Loss in hollow-core optical fibers: mechanisms, scaling rules, and limits," *Advances in Optics and Photonics*, vol. 15, no. 1, pp. 1–85, 2023.
- [3] D. J. Richardson, N. V. Wheeler, Y. Chen *et al.*, "Hollow core fibres and their applications," *Proc. Optical Fiber Comm. Conf.(OFC),Tu3H.1*, pp. 1–80, 2017.
- [4] C. Wei, R. Joseph Weiblen, C. R. Menyuk *et al.*, "Negative curvature fibers," *Advances in Optics and Photonics*, vol. 9, no. 3, pp. 504–561, 2017.
- [5] F. Poletti, M. N. Petrovich, and D. J. Richardson, "Hollow-core photonic bandgap fibers: technology and applications," *Nanophotonics*, vol. 2, no. 5-6, pp. 315–340, 2013.
- [6] M. Petrovich, E. Numkam Fokoua, Y. Chen *et al.*, "Broadband optical fibre with an attenuation lower than 0.1 decibel per kilometre," *Nature Photonics*, vol. 19, no. 11, pp. 1203–1208, 2025. [Online]. Available: <https://doi.org/10.1038/s41566-025-01747-5>
- [7] R. A. Eltaieb, S. Morency, Y. Messaddeq *et al.*, "Impact of bending angle on antiresonant fibers with optimized symmetric geometries," *Optical Fiber Technology*, vol. 90, p. 104071, 2025.
- [8] M. F. Schubert, A. K. Cheung, I. A. Williamson *et al.*, "Inverse design of photonic devices with strict foundry fabrication constraints," *ACS Photonics*, vol. 9, no. 7, pp. 2327–2336, 2022.
- [9] J. Kim, J.-Y. Kim, J. Kim *et al.*, "Inverse design of nanophotonic devices enabled by optimization algorithms and deep learning: recent achievements and future prospects," *Nanophotonics*, vol. 14, no. 2, pp. 121–151, 2025.
- [10] S. H. Fernandez, O. Jovanovic, C. Peucheret *et al.*, "Differentiable machine learning-based modeling for directly-modulated lasers," *IEEE Photonics Technology Letters*, vol. 36, no. 4, pp. 266–269, 2024.
- [11] Z. He, J. Du, X. Chen *et al.*, "Machine learning aided inverse design for few-mode fiber weak-coupling optimization," *Optics Express*, vol. 28, no. 15, pp. 21 668–21 681, 2020.
- [12] F. Meng, J. Ding, Y. Zhao *et al.*, "Artificial intelligence designer for optical fibers: Inverse design of a hollow-core anti-resonant fiber based on a tandem neural network," *Results in Physics*, vol. 46, p. 106310, 2023.
- [13] F. Meng, X. Zhao, J. Ding *et al.*, "Use of machine learning to efficiently predict the confinement loss in anti-resonant hollow-core fiber," *Optics Letters*, vol. 46, no. 6, pp. 1454–1457, 2021.
- [14] Y. Jewani, M. Petry, R. Sanchez-Arias *et al.*, "Accurate loss prediction of realistic hollow-core anti-resonant fibers using machine learning," *IEEE Journal of Selected Topics in Quantum Electronics*, vol. 30, no. 6: Advances and Applications of Hollow-Core Fibers, pp. 1–8, 2024.
- [15] S. Chugh, A. Gulistan, S. Ghosh *et al.*, "Machine learning approach for computing optical properties of a photonic crystal fiber," *Optics Express*, vol. 27, no. 25, pp. 36 414–36 425, 2019.

- [16] H. Kabir, Y. Wang, M. Yu *et al.*, “Neural network inverse modeling and applications to microwave filter design,” *IEEE Transactions on Microwave Theory and Techniques*, vol. 56, no. 4, pp. 867–879, 2008.
- [17] G. Zhenyu, N. Tigang, P. Li, L. Yangmei, L. Jing, Z. Jingjing, S. Jingyi, Z. Chengbao, W. Hua, J. Wei *et al.*, “Confinement loss prediction in diverse anti-resonant fibers through neural networks,” *Optics Express*, vol. 32, no. 6, pp. 8903–8918, 2024.
- [18] T. Hastie *et al.*, “The elements of statistical learning: data mining, inference and prediction,” *The Mathematical Intelligencer*, vol. 27, no. 2, pp. 83–85, 2005.